Joint product state distribution of coincidently generated photofragment pairs

K.-H. Gericke, H. G. Gläser, C. Maul, and F. J. Comes
Institut für Physikalische und Theoretische Chemie, Niederurseler Hang, D 6000 Frankfurt am Main 50, Federal Republic of Germany

(Received 16 June 1989; accepted 20 September 1989)

The joint product state distribution of coincident fragment pairs formed in the same elementary photodissociation process has been determined. This correlation between quantum state populations of two molecular products has been measured by high resolution Doppler spectroscopy in conjunction with level-specific detection of the ejected photofragments. One product molecule, formed in a specific quantum state, is excited by laser induced fluorescence and the wing of the corresponding Doppler profile is analyzed to determine the product state distribution of the partner fragment. In the photodissociation of jet-cooled hydrogen peroxide at 193 nm two OH partner radicals are formed with comparable angular momenta. For a specific rotation of one hydroxyl radical the product state distribution of the partner fragment is centered at about the same rotation with a width of only a few rotational quanta. The orbital angular momentum is of the order of 1 $\hbar$ and the impact parameter is extremely small. Experimentally observed joint product state distribution and trajectory calculations on *ab initio* potential energy surfaces are in excellent agreement.

I. INTRODUCTION

The understanding of dissociation dynamics has significantly increased by the quantitative determination of directional properties and their mutual correlations.[1-3] Since the products probe the excited state potential energy surface from the Franck–Condon exited region to the asymptotic region a characterization of the upper potential becomes feasible by a measure of the correlation between the translational **v** and rotational **J** motion of the fragment because this $\langle \mathbf{v}\cdot\mathbf{J} \rangle$ correlation is related to the gradients of the repulsive force exerted in the dissociation process and is independent on parent molecule motion. Another important correlation of linear molecular fragments with vanishing angular momentum projection along the molecular symmetry axis is the population of Λ doublet states[4-6] which reflects the symmetry restriction of the fragmentation process. The unequal population of spin–orbit states also reveals the geometry of chemical events.[6-9]

All of these correlations are related to each of the product molecules, but only limited information is available about an interrelation *between* the two products generated in the same elementary event of photodissociation.

In the photofragmentation of CH_3ONO a Fourier transform inversion procedure has been applied to analyze the energy pair correlation of the NO and CH_3O fragments.[10] The method provides a rough view over the distribution of the CH_3O products for particular state-selected NO partner molecules. It was shown that the internal energy distribution of the CH_3O fragment is approximately Gaussian, with no evidence for any energy correlation between the two products.

The photodissociation of HF dimers has been investigated by measuring fragment angular distributions using a rotatable molecular beam apparatus.[11] The distribution shows some structure which is composed of a superposition of individual rotational excited fragment channels. The data could be used to establish the existence of intermolecular energy correlations between the rotational states of both HF partner molecules.

In the photodissociation of cyanogen the observation of angular and velocity distributions of state resolved fragments gave some information about correlations between the rotation of the products.[12] The velocity distribution showed that with increasing rotation of the selected fragment the velocity distribution narrows.

In a preceding paper only the average rotational energy of the OH (OD) partner molecules coincidently formed in the fragmentation of H_2O_2 (D_2O_2) at 266 and 193 nm was measured by evaluation of Doppler profiles.[13,14] For a nonrotating parent both OH (or OD) partner products are ejected on the average with the same rotation, i.e., the rotational angular momenta $J(OH_A)$ and $J(OH_B)$ of the molecular products $OH_A + OH_B$ are strongly correlated. Dixon *et al.*[15] measured the average OH pair correlation at a photolysis wavelength of 266 nm in an effusive H_2O_2 beam using velocity-aligned Doppler spectroscopy.[16] It was also found that the mean rotational energy of the partner OH increases linearly with that of the probed OH. However, in none of these experiments the complete state-selected joint reaction probability $P(J_A,J_B,)$ has been measured.

The present paper reports on an investigation of coincident product pair formation in the photodissociation of hydrogen peroxide at 193 nm where the initial parent motion is either Boltzmann distributed at $T = 300$ K or cooled in a supersonic jet. The probability matrix $P(J_A,J_B)$ has been determined by measuring the wings of Doppler broadened line shapes with a high resolution dye laser system.

II. DETERMINATION OF PAIR CORRELATIONS

The dissociation process

$$AB + h\nu \rightarrow A(q_A) + B(q_B) + \Delta E(q_A,q_B),$$

 0021-9606/90/010411-09$03.00

where the product molecules A and B are ejected in specific quantum states q_A and q_B, is subject to several constraints which limit the recoil velocity and allow an evaluation of the joint reaction probability $P(q_A,q_B)$.[17] Since the total linear momentum has to be zero in the center of mass system, the total kinetic energy of both fragments is simply given by

$$E_{kin} = E_{kin}(A) + E_{kin}(B)$$
$$= \tfrac{1}{2}\mu v_{AB}^2 = \tfrac{1}{2}m_A(1 + m_A/m_B)v_A^2, \quad (1)$$

where the symbols have the usual meaning. Conservation of energy leads to an equation which allows a determination of the internal energy $E_{int}(B)$ of fragment B when the partner product A is formed with the internal energy $E_{int}(A)$,

$$E_{int}(B) = E_{av} - E_{int}(A) - E_{kin}, \quad (2)$$

where the available energy E_{av} is determined by the photon energy $E_{h\nu}$, the dissociation energy E_D, and the internal energy of the parent $E_{int}(AB)$,

$$E_{av} = E_{h\nu} + E_{int}(AB) - E_D. \quad (3)$$

For a fixed value of the available energy, the internal energy of product B can be determined by accurate measurement of the velocity v_A of the partner fragment A which is generated in the same dissociation process,

$$E_{int}(B) = E_{av} - E_{int}(A) - \tfrac{1}{2}m_A^2\, v_A^2/\mu. \quad (4)$$

To resolve the complete product state distribution of fragment pairs, the velocity v_A has to be measured with an accuracy δv_A,

$$\delta v_A \leqslant \delta E_i \frac{v_A}{2[E_{av} - E_{int}(A) - E_{int}(B)]}, \quad (5)$$

where δE_i represents the uncertainty of $E_{h\nu}$, E_D, $E_{int}(AB)$, $E_{int}(A)$, and in the energetic difference between two quantum states of the fragment B.

The velocity v_A can be measured very accurately by Doppler spectroscopy using the laser induced fluorescence technique (LIF) in connection with a dye laser system of sufficiently high resolution. The internal energy of the product A, $E_{int}(A)$, is well known from the term value of the initial level probed by LIF, the photolysis energy is very sharp when lasers are used as light sources, and the internal energy of the parent can strongly be reduced by cooling in a supersonic jet. The dissociation energy E_D is usually well known or can be measured by the amount of energy which is partitioned among the different degrees of freedom.[17]

For an elementary dissociation process the intensity of a spectral line as a function of frequency is given by[2]

$$I(\nu) = C\sum_{q_B}\frac{P(q_A,q_B)}{2\Delta\nu_D}\left[1 + \beta_{eff}P_2\left(\frac{\nu-\nu_0}{\Delta\nu_D}\right)\right]$$
$$\text{for } |\nu-\nu_0| \leqslant \Delta\nu_D, \quad (6)$$

where $P_2(x)$ is the second Legendre polynomial, $P_2(x) = \frac{3}{2}x^2 - \frac{1}{2}$, and β_{eff} is the effective anisotropy parameter which contains all information of vector correlations existing in the dissociation process. The fragment velocity can be determined from the maximum Doppler shift $\Delta\nu_D$.

If the dissociation process is completely isotropic, i.e., $\beta_{eff} = 0$, then Eq. (6) reduces to a sum of rectangular profiles which are only smeared out by the experimental laser line width and residual parent translational motion.[2]

In general, β_{eff} is not zero, but can be diminished by suitable combination of profiles obtained at different geometries and transitions.[18] The influence of a spatial anisotropic fragmentation on the Doppler line will also be eliminated if the "magic" observation angle geometry with $\theta_m = 54.7°$ is chosen.[14] Hence, only a correlation between the translational and rotational motion of the product will modify the (rectangular) Doppler profile. However, the evaluation of the broadened lines in terms of coincident product pairs will only be influenced to a minor extent by this anisotropy, if a transition is chosen where the wing of the line is sharp and not smeared out by a $\langle \mathbf{v}\cdot\mathbf{J}\rangle$ correlation. This can always be achieved if a P or R branch is excited when $\mathbf{v}$ is more perpendicular to $\mathbf{J}$ or if a Q transition is probed in the case of $\mathbf{v}$ being more parallel to $\mathbf{J}$. Therefore, the line function can be regarded as a sum of rectangular Doppler profiles, where the weighting of each rectangle is related to $P(q_A,q_B)$,

$$I \sim \sum_{q_B}\frac{P(q_A,q_B)}{2\Delta\nu_D}\Theta(\Delta\nu_D - |\nu-\nu_0|). \quad (7)$$

$\Theta(x)$ is the step function; $\Theta(x \geqslant 0) = 1$, $\Theta(x<0) = 0$.

The velocity, respectively the Doppler width of a line at center frequency ν_0 ($v = \Delta\nu_D c/\nu_0$), is quantized as a consequence of the quantization of the partner product's energy and all other energies are assumed to be well defined. The required resolution $\delta\nu_l$ of the analyzing dye laser is given by

$$\delta\nu_l \leqslant \delta E_i(\nu_0/c)/m_A$$
$$\times\{2[E_{av} - E_{int}(A) - E_{int}(B)]/\mu\}^{-1/2}. \quad (8)$$

In the special case of H_2O_2 photodissociation at 193 nm two OH ($X^2\Pi$) products are ejected which are rotationally excited only.[3,19] The maximum of rotation is close to $J_{OH} \cong 12$ corresponding to an internal energy of $E_{int} \cong 2850\ cm^{-1}$. The energy spacing to the next rotational state $J_{OH} = 13$ is roughly $500\ cm^{-1}$.[20] If the OH radicals are probed by the $A^2\Sigma^+(v'=0,J') \leftarrow X^2\Pi(v''=0,J'')$ transitions around 314 nm [$P_1(12)$ line[27]], the detection of an energy spacing of $\delta E_i = 500\ cm^{-1}$ demands a line width of the analyzing dye laser of $\delta\nu_l \lesssim 120$ MHz. All remaining uncertainties in energies, like the spectral width of the photolyzing laser, will smear out the Doppler profile and should consequently be kept well below $500\ cm^{-1}$.

III. EXPERIMENTAL

The OH product pairs are analyzed by Doppler spectroscopy using LIF as diagnostic tool. Any influence of initial parent motion on the shape of the fragment absorption line has to be minimized. An adequate experimental procedure is the use of the molecular beam technique. The basic experimental setup is shown in Fig. 1. The reaction chamber is made of stainless steel and evacuated by a 360 ℓ/s turbo molecular pump (Turbovac 360 CSV, Leybold–Heraeus) which produce a basic pressure of less than 10^{-3} Pa.

A molecular beam of hydrogen peroxide was generated by bubbling helium or argon through liquid H_2O_2/H_2O (95% H_2O_2) and expanding the mixture through a pulsed

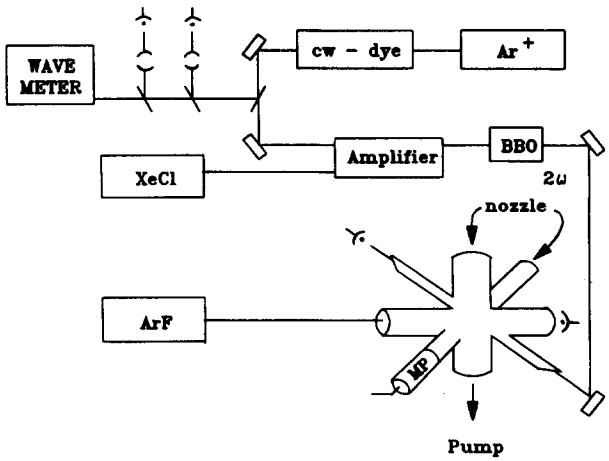

FIG. 1. Schematic diagram of the experimental set up.

nozzle. The aperture of the nozzle system was 1 mm in diameter and the final pulse length was adjustable from 200 μs to 10 ms which was monitored by a fast ionization gauge (response time $< 10\,\mu$s). The mean background pressure in the vacuum chamber was well below 0.1 Pa at a repetition rate of 20 Hz.

The H_2O_2 molecules were photolyzed 2 cm downstream by the light of an ArF excimer laser (Lambda Physik, 101 MSC) at 193 nm. The spectral emission width of this laser is less than 1 nm corresponding to an uncertainty of $\delta E_{h\nu} = 260\ \mathrm{cm}^{-1}$. The beam was aligned and focused by a plan and a spherical dielectric mirror ($R = 1$ m) to a spot size of $\sim$2mm. The influence of stray light from the entrance window was reduced by the use of a series of light baffles.

Doppler profiles were analyzed by LIF probing OH absorption lines of the P branch of the $A\,^2\Sigma^+(v'=0) \leftarrow X\,^2\Pi(v''=0)$ electronic transition. The probe laser system consists of a single mode ring laser (CR 699-21, Coherent) pumped by an argon ion laser (Innova 100, Coherent). With a pump power of 5 W at 514.5 nm a single mode output power of 0.5 W was achieved using rhodamin B as active laser material. The band width of the radiation is better than the detected 2 MHz, which is the maximum resolution of an external confocal Fabry–Perot interferometer (300 MHz free spectral range).

The tuning range at this bandwidth is limited to 30 GHz in the visible which is sufficient to scan a complete Doppler profile. A minor part of the dye laser beam is splitted by a quartz flat in order to monitor the emitted wavelength, band width, detuning, and relative output power. The wavelength of the dye laser is controlled by an accurate wave meter (WA 20-VIS, Burleigh Instruments) with a resolution of better than 1 GHz which allows a simple "wavelength positioning" of the analyzing laser.

Two spectrum analyzers (Coherent) measure the tuning of the dye laser. The first one has a free spectral range of 1.5 GHz and a finesse of 200. This analyzer is used as a frequency marker when the complete Doppler line is recorded. In order to measure the wing of a profile the scanning range of the ring laser (1.5–2 GHz) is controlled by the second confocal Fabry–Perot interferometer which exhibits a free spectral range of 300 MHz and a finesse of better than 150. Since the spectrum analyzers are used as frequency markers to eliminate nonlinearity in the tuning of the ring laser, the free spectral range has to be known very accurately. Therefore, we set up an experiment where selected small parts of the visible I_2 spectrum were monitored and the relative position of the iodine lines were compared with the frequency markes of both Fabry–Perot interferometers.[22] Within the experimental error of $< 0.5\%$ which was mainly caused by the uncertainty of I_2 line positions the measured free spectral ranges agree with the values stated previously.

After passing a delay line of $\sim$5 m the cw ring laser beam was amplified in a three stage dye amplifier (FL 2003, Lambda Physik; rhodamine 101 dissolved in methanol) which was pumped by a XeCl excimer laser (Lambda Physik) at 308 nm. The temporal and spectral width of the dye laser beam depends on the pulse length of the excimer laser. Three excimer lasers with different pulse length have been tested to obtain tunable light pulses with maximum output power and minimum spectral width.

The first tested XeCl laser delivered 150 mJ at a pulse length of 15 ns. An output energy of the amplified dye of more than 5 mJ was obtained without excessive alignment procedures. The band width was measured to be 80 MHz using one of the spectrum analyzers (FSR 1.5 GHz). Since the dye laser can only operate in the visible but the required radiation to excite the $OH(A\,^2\Sigma^+ \leftarrow X\,^2\Pi)$ electronic transition is about 314 nm, the tunable radiation has to be frequency doubled which further increases the bandwidth by a factor between $\sqrt{2}$ and 2, corresponding to the regime of quadratic or linear power dependence of conversion. Thus, a spectral width of at least 120 MHz has to be expected in the UV in that case.

The second system was a special long pulse excimer laser producing 200 mJ pulses at a length of 200 ns. Due to the nonlinear behavior between the pump power and the amplified dye radiation, the pulse length of the dye laser is strongly reduced to $\cong$50 ns resulting in a spectral width of better than 20 MHz at an output energy of less than 0.5 mJ.

The XeCl excimer which was finally used to determine the OH angular momentum correlations delivered pulses with a length of 55 ns at an energy of up to 200 mJ. The pulse duration of the amplified light of the cw ring laser was reduced to about 25 ns and the Fourier-limited spectral width was measured to be 30 MHz at an output energy of 5 mJ. A BBO crystal doubles the frequency of the pulsed dye laser radiation with an efficiency of approximately 10%. The energy of the second harmonic varies only to a minor extent over the tuning range of 60 GHz in the UV. Therefore, a scan of the dye laser can be performed without angle tuning of the BBO crystal. The dye laser beam enters the reaction chamber under the "magic angle" geometry, i.e., at an angle of 54.7° between the analyzing and photolyzing laser beams in order to minimize the influence of translational anisotropy on the Doppler profiles.

The LIF signal was viewed perpendicular to the plane formed by the two laser beams with a photomultiplier tube

(Valvo) equipped with f 1.0 imaging optics and an interference filter (310 ± 10 nm), but without the use of polarizers. Photomultiplier output was measured with a boxcar integrator (Stanford, SRS 250) and stored in a microcomputer after A/D conversion. The pulse energies of both laser beams were monitored by two Si detectors. The signals were directly A/D converted and also registered in the computer. So the fluorescence signal could be normalized with respect to the photolysis and probe laser energies on a shot to shot basis. Scanning of the dye laser was performed by the computer after D/A conversion and controlled by the spectrum analyzers. A four channel trigger device (DG 535, Stanford) controlled all time events in the experiment. The delay between the photodissociation excimer laser and the dye laser was set to 20 ns determined by the pulse length and jitter of the excimer lasers. Gate duration was 800 ns placed 20 ns after the probe laser pulse. In order to obtain maximum cooling conditions the photolysis laser pulse was adjusted to overlap with the density maximum of the gas pulse.

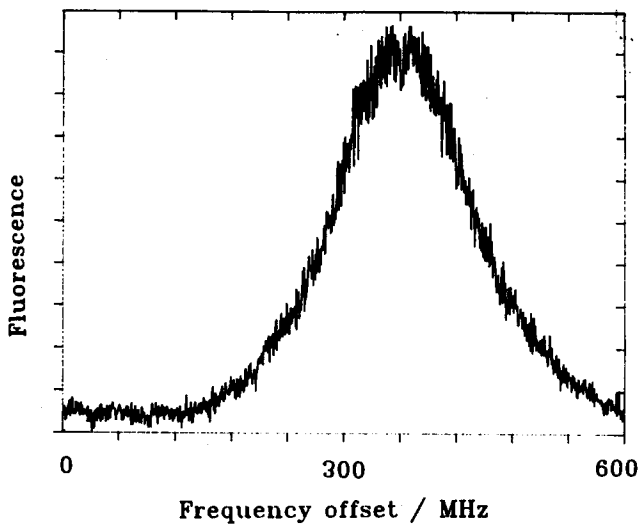

FIG. 2. Observation of a isolated transition of pyrazine of the 0_0^0 band in the ${}^1B_{3a} \leftarrow {}^1A_{1g}$ electronic system in order to determine the translational cooling in the molecular beam.

IV. RESULTS

In this type of experiment where energy pair correlations are measured one has to consider the limited resolution of the dye laser system, the internal energy spread of the parent, and the initial translational motion which will superpose the recoil velocity. All these effects will contribute to the final Doppler width. Without considerable reduction of the experimental broadening of the absorption line the wings of the Doppler profiles would be indistinct and structureless. The internal energy of H_2O_2 at room temperature is mainly determined by parent molecule rotation and only to a minor extent by the torsional OH vibration. In total, $E_{\text{int}}(H_2O_2) \simeq 400\,\text{cm}^{-1}$ has to be considered when thermal ($T = 3300$ K) hydrogen peroxide is photolyzed. Although this uncertainty in energy restricts the accuracy in the measurement of product pair correlations, the main limitation is caused by translational motion of the parent. At room temperature, the OH Doppler width will be about $\Delta\nu_D(H_2O_2) = 2$ GHz and, therefore, becomes much larger than the required resolution. Thus, the parent molecules have to be cooled down in a molecular beam.

Since the translational temperature of H_2O_2 in a molecular beam cannot be measured by simple spectroscopic methods, the cooling of pyrazine (1,4-Diazin) under comparable conditions was determined. The spectral width of a single separated line in the 0_0^0 band of the ${}^1B_{3u} \leftarrow {}^1A_{1g}$ system near 30 873.2 cm^{-1} has been measured at a stagnation pressure prior to expansion of 4×10^4 Pa argon (Fig. 2).[23] The measured line width of 140 MHz is composed by the laser band width, $\Delta\nu_l \cong 50$ MHz, the spectral width of the transition characterized by the lifetime ($\tau \cong 100$ ns, $\Delta\nu_s \cong 10$ MHz), and the residual Doppler shift $\Delta\nu_D$ due to the remaining translational temperature. Since the translational cooling of hydrogen peroxide should be comparable to that of pyrazine (1,4-Diazin), a similar spectral uncertainty is expected. Lower translational temperatures can be obtained by higher stagnation pressure. However, the relatively high density in this molecular beam has to be taken into account, because the photofragments are ejected with high velocities which are uncorrelated with the beam direction. In order to exclude perturbations by subsequent collisions during the time of interrogation the OH Doppler width of low rotational states was monitored at different nozzle stagnation pressures and delay times. Any translational and/or rotational relaxation will cause an increase of LIF intensity in the center of the profile. Since the observed translational relaxation of OH fragments is very fast, the optimum nozzle conditions are always a compromise between very effective parent cooling and collisions of the products with the inert gas.

The observed OH product rotational state distribution can be characterized by Gaussian distribution peaking at $J_{\text{OH}} = 12$ with a width at half-maximum of $\Delta J_{\text{OH}} \cong 4$ when jet-cooled hydrogen peroxide is photolyzed. Photodissociation of H_2O_2 at room temperature in bulk results in the same kind of distribution, but with a width of $\Delta J_{\text{OH}} \cong 6$.[19] Quantum states probed were ranging from $J_A = 7$ to 16 for jet-cooled hydrogen peroxide. In order to determine the pair correlations OH Doppler profiles were first recorded in a fast 60 GHz scan. An example of such a scan is shown in Fig. 3 together with frequency markers of the spectrum analyzer. After frequency correction of the recorded line profile the parameters of Eq. (9) were fit to the data with suitable convolution of a Gaussian function

$$I(\nu_1) = C \int_{-\infty}^{+\infty} \exp\left[-\left(\frac{\nu - \nu_1}{\Delta\nu_a}\right)^2\right] \times \left[1 + \beta_{\text{eff}} P_2\left(\frac{\nu - \nu_0}{\Delta\nu_D}\right)\right] d\nu + B. \quad (9)$$

According to this procedure the center of the line ν_0 the mean Doppler width $\Delta\nu_D$, and the β_{eff} parameter are obtained very accurately.

Figure 4 shows the mean rotational state $\langle J_B \rangle$, obtained from the mean line width of OH_A product, formed coincidently with OH_A in a particular rotational state J_A. Obvi-

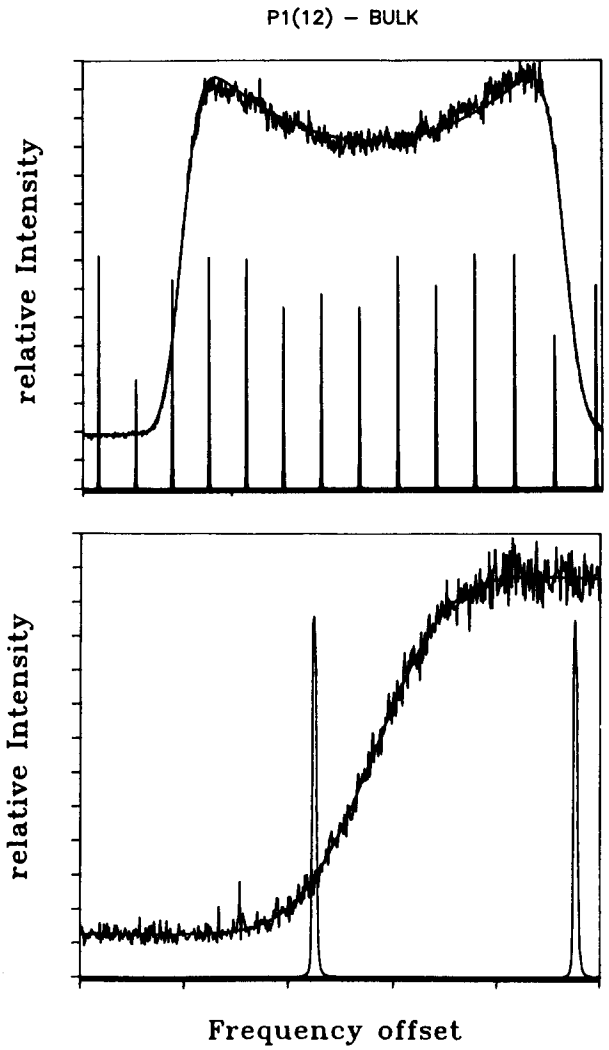

FIG. 3. Recoil Doppler broadened line profiles of the $P_1(12)$ transition when jet-cooled hydrogen peroxide is photolyzed at 193 nm. The solid line represents a Gaussian fit to the data, obtained by a least-squares-fit procedure.

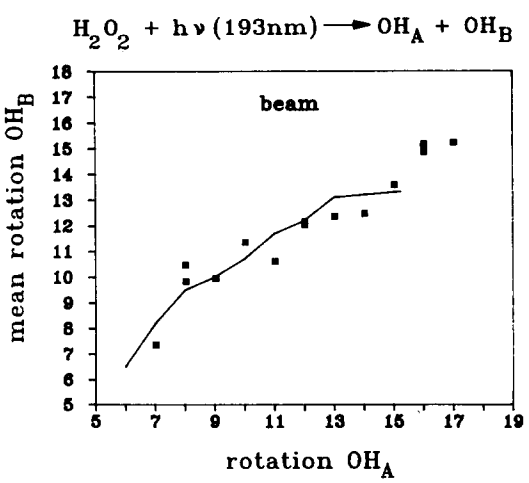

FIG. 4. Correlation between the angular momentum J_A of fragment OH_A and the mean rotation $\langle J_B \rangle$ of the partner product OH_B. The solid curve is the result of trajectory calculations performed by Schinke (Ref. 27).

ously the excitation of cold H_2O_2 parent molecules at 193 nm leads to a strong correlation between the angular momenta of coincident product pair: $J_A \cong \langle J_B \rangle$. The *partner* state distribution can be evaluated from the wings of the Doppler profiles. Therefore, this part of the line profile was separately scanned with higher resolution and a step size of 6–10 MHz per data point.

In principle, a fit of Eq. (6) with suitable convolution of the laser band width and residual parent molecule motion to the wings of a Doppler profile will yield the partner distribution q_B of fragment B. But in the case of OH products the special character of the $^2\Pi \leftarrow {}^2\Sigma$ transition has to be considered. The nuclear spin of the H atom interacts with the spin of the electron and splits each level. The spacing of such a doublet is about 50 MHz in the $^2\Pi$ electronic ground state.[24] However, the interaction of the unpaired electron spin density of a $^2\Sigma^+$ state with the magnetic moment of the H nucleus is strongly increased and the Hamiltonian for the $A\,^2\Sigma^+$ state can be written as

$$H_{hf} = b(\mathbf{I}\cdot\mathbf{S}) + cI_zS_z. \tag{10}$$

The hyperfine coupling constants b and c have been measured by ter Meulen *et al.*[25] to be $b = 722.5$ MHz and $c = 165.8$ MHz. For higher $OH(^2\Sigma^+)$ rotations, the splitting becomes almost independent of J and the spin orbit state. For $J' \geqslant 7$ a constant splitting of 360 MHz is calculated. The deviation from the exact splitting is less than 10 MHz and, therefore, negligible in the analysis of OH Doppler profiles.

As a consequence of the hyperfine splitting each line may be composed of up to four transitions. The transition probabilities are listed in Table I. Because of the selection rules $\Delta F = 0, \pm 1$ the lines of the P and R branches are composed of three different transitions only. However, for $J'' \geqslant 7$ only two main transitions contribute significantly to the line profile. These are the transitions which follow the selection rule $\Delta F = -1$ for the P branch, $\Delta F = 0$ for the Q branch, and $\Delta F = +1$ for the R branch. The corresponding relative transition probabilities are close to 0.5, with a contribution of the satellite transitions of less than 1%.[26]

In the analysis of the Doppler profiles of the P branch the splitting into two different lines is considered. The spectral separation of both transitions is the difference between the hyperfine splitting of the $A\,^2\Sigma^+$ state and the $X\,^2\Pi$ electronic ground state. Thus, for higher OH rotations each line is composed of two transitions which have the same transition probability and are separated by ~310 MHz. A fit of a sum of these two lines according to Eq. (6) to the wing of a Doppler profile gives the partner product distribution $P(J_AJ_B)$. The two parameters β_{eff} and v_0 are taken from the measurement of the total Doppler line. The bars in Fig. 5 depict the *partner* state distribution $P(J_AJ_B)$ for the product OH_B when the partner OH_A is formed in a specific rotational state J_A. The points in Fig. 5 are the result of trajectory calculations on an *ab initio* potential energy surface performed by Schinke.[27,28] The solid line is drawn to obtain a better visual impression of the calculated distribution since the accuracy of some data points is limited as a consequence of an insufficient number of trajectories. All distributions are normalized to the peak value. The J_B distributions for pho-

TABLE I. Relative transition probabilities between hyperfine levels of the OH ($A^2\Sigma^+ \leftarrow X^2\Pi$) system.

Branch	F'	$F' = J'' - 1/2$	$F'' = J'' + 1/2$
P_1, P_2, O_{12}, Q_{21}	$J'' - 3/2$	$\frac{J''-1}{2J''-1}$	0
$J' = J'' - 1$	$J'' - 1/2$	$\frac{1}{4J''^2-1}$	$\frac{J''+1}{2J''+1}$
Q_1, Q_2, P_{12}, R_{21}	$J'' - 1/2$	$\frac{(2J''-1)(J''+1)}{(2J''+1)^2}$	$\frac{1}{(2J''+1)^2}$
$J' = J''$	$J'' + 1/2$	$\frac{1}{(2J''+1)^2}$	$\frac{J''(2J''+3)}{(2J''+1)^2}$
R_1, R_2, Q_{12}, S_{21}	$J'' + 1/2$	$\frac{J''}{2J''+1}$	$\frac{1}{(2J''+1)(2J''+3)}$
$J' = J'' + 1$	$J'' + 3/2$	0	$\frac{J''+2}{2J''+3}$

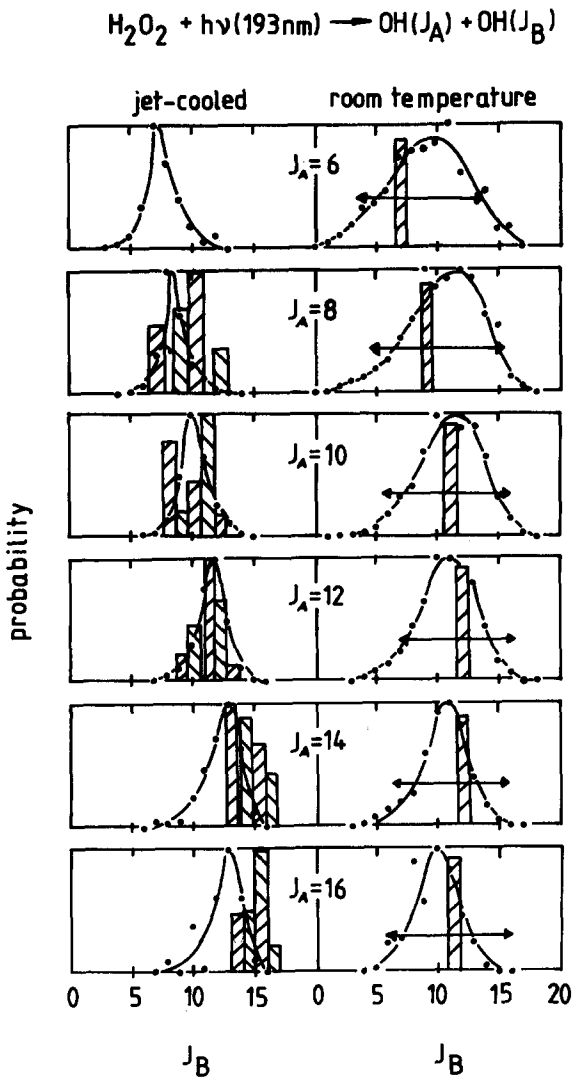

FIG. 5. Product pair distribution of OH_A and OH_B formed in the photodissociation of jet cooled or room temperature H_2O_2. Shown is the rotational distribution of fragment OH_B for a fixed rotational state J_A of partner product OH_A. The solid curve and the data points are the result of trajectory calculations performed by Schinke (Ref. 27). The bars represent the measured distribution. The distributions are normalized to their maximum values. For thermal H_2O_2 ($T = 300$ K) only the center and the width was determined.

tolysis of jet-cooled H_2O_2 are very narrow for all J_A. The width is about 3 $\hbar$ and the peak is very close to $J_B, J_A \cong J_B$.

The photodissociation of thermal H_2O_2 leads to a much broader partner state distribution and the peak shifts only slightly to higher J_B with increasing J_A. The distribution cannot be resolved experimentally because of the residual H_2O_2 Doppler motion. The width and the center of the distribution can only be determined. The rotation of the two OH partner products is highly correlated for low internal parent excitation, but almost vanishes at higher temperature, due to rotational motion of hydrogen peroxide. The results of thermal H_2O_2 photolysis agree with preliminary observations using a low resolution dye laser.[13]

V. DISCUSSION

The most detailed information about a chemical process is contained in the joint microscopic probability matrix $P(q_A, q_B)$ which has to be known to elucidate the dynamics of the process. In case of photodissociation of H_2O_2 at 193 nm both partner products are chemically identical. However, there is *a priori* no reason that the two fragments are generated with the same amount of angular momentum. If the two partner products are completely uncorrelated, the probability matrix is simply given by the product of the traditionally measured product distributions $P_A(J_A)$ and $P_B(J_B)$:

$$P(J_A, J_B) = P_A(J_A) \cdot P_B(J_B). \tag{11}$$

Since the probability matrix $P(J_A, J_B)$ has to be symmetric for identical products

$$P(J_A J_B) = P(J_B, J_A) \tag{12}$$

the probabilities $P_A(J_A)$ and $P_B(J_B)$ are also identical

$$P_A(J_A) = \sum_{J_B} P(J_A, J_B) = \sum_{J_A} P(J_B, J_A) = P_B(J_B). \tag{13}$$

On the other hand, a complete correlation between both products ($J_A = J_B$) leads to the probability matrix

$$P(J_A, J_B) = \delta_{J_A, J_B} \cdot P(J_A). \tag{14}$$

In both cases, in the completely uncorrelated fragmentation

probability or in the strictly correlated one, it is sufficient to measure $P_A(J_A)$— and $P_B(J_B)$ for chemically different products—to obtain the maximum information about the dissociation process. However, a knowledge of $P_A(J_A)$ and $P_B(J_B)$ is insufficient to decide whether one of these extremes is reached or not. Thus, a decision can only be passed when the matrix $P(J_A,J_B)$ is measured.

Figure 6 shows the complete joint reaction probability matrix where the weighting of the measured $P(J_A,J_B)$ is performed by the well known rotational state distribution $P(J_A)$[19] shown on the left area of the diagram. A good check of the reliability of the data is the calculation of $P_B(J_B) = \Sigma_{J_A} P(J_A,J_B)$ which should give an identical product state distribution. The result of such a calculation depicted on the right projection area of Fig. 6 shows satisfying conformity with the expected distribution. The value of $P(J_A = 10,J_B)$ is probably not a dynamical feature but caused by uncovered perturbations during the experiment.

The OH pair correlation can be caused dynamically by bending motion associated with the two O–O–H angles and by torsional motion of the two OH rotamers. With increasing temperature the H_2O_2 parent rotation breaks the symmetry in the lab frame and the pair correlation will be reduced. Especially parent rotation about the a-inertial axis (essentially the O–O bond) will influence the rotation of the OH pairs which leads to a broadening of the J_B distribution for any selected rotational state J_B (right-hand side of Fig. 5). Therefore, it is recommended to use cold parent molecules in order to gain maximum insight into the intramolecular dynamics from pair correlation measurements.

If OH rotation would be generated exclusively from bending motion by strong O–O repulsion J would be perpendicular to v, whereas a parallel orientation between the translational and rotational motion of the OH fragment points at a torsional dependence of the excited state potential. Experimentally a very strong positive correlation between v and J is observed, indicating a preferentially parallel alignment between these directed properties.[19] Thus, the OH pair rotation is essentially generated via torsional motion of the OH rotors during fragmentation. As a consequence the rotational energy of the partner molecules has to be the same, and the rotational vectors point into opposite direction, $\mathbf{J}_A = -\mathbf{J}_B$, due to conservation of angular momentum.

Any deviation from this strong *vectorial* pair correlation, $\mathbf{J}_A = -\mathbf{J}_B$, is caused by bending motions of the two OH rotamers. In the photolysis of jet cooled H_2O_2 at 193 nm we obtained an expectation value of the squared angular momentum components[19]:

$$f_{\text{torsion}} = \langle J^2_{\text{torsion}} \rangle / J(J+1) \cong 0.7. \tag{15}$$

Without the influence of bending motion the joint reaction probability matrix [Eq. (14)] is diagonal. The deviations of the observed matrix $P(J_A,J_B)$ shown in Fig. 6 from the diagonal elements therefore reflect the influence of bending motion. The fraction of OH rotational energy in the different modes is calculated according to the following equation:

$$f_{\text{bend}} = \frac{\Sigma_{J_B \neq J_A} P(J_A,J_B)\,|E_r(J_A) - E_r(J_B)|}{\Sigma_{J_B} P(J_A,J_B) E_r(J_B)}$$

$$f_{\text{torsion}} = 1 - f_{\text{bend}}. \tag{16}$$

Figure 7 shows the fraction of OH rotation (full circles) which originates from torsional motion as a function of the angular momentum. On the average only 20% of OH rotation originates from bending motion and 80% of OH rota-

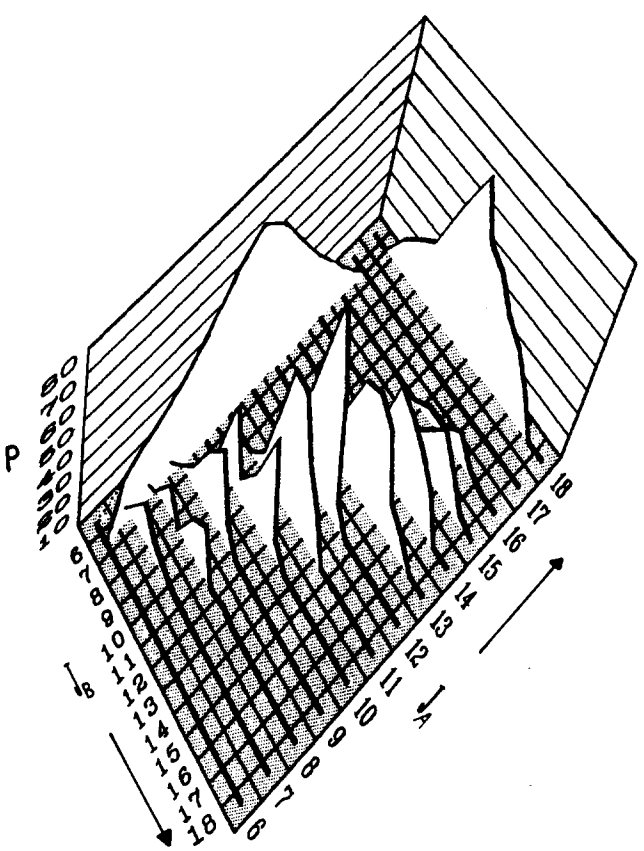

FIG. 6. Complete microscopic joint reaction probability $P(J_A,J_B)$ for the photodissociation of H_2O_2 at 193 nm. The traditionally product state distribution $P(J)$ is obtained by summing up all partner contributions.

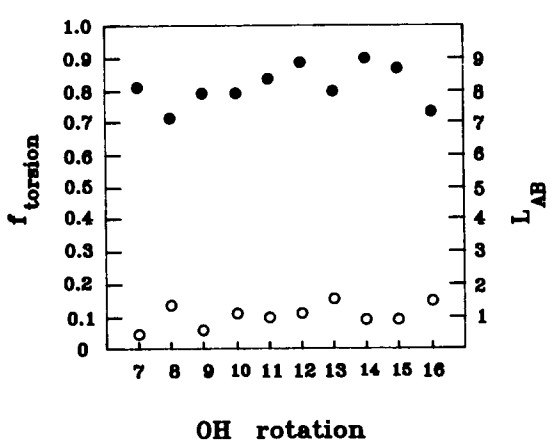

FIG. 7. Fraction of OH rotation f_{torsion} which is generated by torsional motion of the two rotamers (filled circles) and orbital angular momentum L_{AB} (open circles) which compensates any deviation from an antiparallel orientation between $\mathbf{J}_A$ and $\mathbf{J}_B$.

tion is generated via a torsional dependence of the upper potential surface which is slightly more than the value obtained by vector correlation measurements. A small deviation is not surprising because Eq. (16) counts all product pair correlations which have the same amount or rotation, $|\mathbf{J}_A| = |\mathbf{J}_B|$, i.e., both a parallel orientation between $\mathbf{J}_A$ and $\mathbf{J}_B$ and an antiparallel orientation, $\mathbf{J}_A = -\mathbf{J}_B$, are considered, whereas the positive $\langle \mathbf{v}\cdot\mathbf{J} \rangle$ vector correlation implies an opposite direction of the angular momenta. A value of $f_{\text{torsion}} = 0.8$ corresponds to an average angle between $\mathbf{v}$ and $\mathbf{J}$ of $\alpha_{vJ} \cong 26°$.

Included in Fig. 7 is the mean deviation of pair rotation $\Delta J = |J_A - J_B|$, from the diagonal relation $J_A = J_B$:

$$\langle \Delta J \rangle = \sum_{J_B} P(J_A, J_B) |J_A - J_B| / P(J_A). \tag{17}$$

There is no significant variation of f_{torsion} and $\langle \Delta J \rangle$ with OH product rotation and the value of $\langle \Delta J \rangle$ is in the order of 1 $\hbar$.

From the detailed knowledge of the product pair rotations information about the orbital angular momentum L_{AB} and the impact parameter b can be extracted. In general, conservation of angular momentum limits the range of the orbital angular momentum for a nonrotating parent to

$$J_A + J_B \geqslant L_{AB} \geqslant |J_A - J_B|. \tag{18}$$

Furthermore, the available phase space is also limited by energy conservation

$$L_{AB} = b\sqrt{2\mu[E_{av} - E_{int}(A) - E_{int}(B)]}, \tag{19}$$

where the relation

$$L_{AB} = \mu b v_{AB}. \tag{20}$$

is used, with μ being the reduced mass of the A–B system and v_{AB} the relative velocity of products A and B.

In the photodissociation of H_2O_2 at 193 nm we observe large values for J_A and J_B. Since Eq. (18) has to be fulfilled for each elementary process and the partner distributions are known, L_{AB} can take a wide range of values, $2J \geqslant L_{AB} \geqslant 0$, and even large values for the impact parameter b are possible. This situation is shown in Fig. 8 where b [Eq. (20)] is plotted as a function of product rotation J and orbital angular momentum L_{AB}. However, from the vector correlation measurements we know that $\mathbf{J}_A$ and $\mathbf{J}_B$ are essentially antiparallel and consequently $L_{AB} = 0$ for $\mathbf{J}_A = -\mathbf{J}_B$. Only the small amount of rotation which deviates from $J_A = J_B$ has to be compensated by L_{AB} to fulfill the conservation of angular momentum. Thus, the quantity ΔJ is a measure of the orbital angular momentum L_{AB}. From Eq. (20) the impact parameter of the dissociation process can be calculated as a function of rotational states

$$b = L_{AB}(J)/\mu v_{AB}(J) = \frac{\Delta J \nu_0}{\Delta \nu_D c m_{OH}}. \tag{21}$$

The calculated impact parameter does not vary significantly with product rotation and an extremely small average impact parameter of $b = (1.0 \pm 0.3)$ pm is calculated. This is even less than the distance between the OH center of mass to the oxygen atom. Thus, the acting force which separates the two OH fragments during the dissociation process is not directed exactly between the two oxygen atoms but the repulsion takes place more between the two OH center-of-mass systems and the simple picture of O–O repulsion is completely insufficient to describe the dissociation of hydrogen peroxide. The reaction pass of the fragments elapses on several coordinates of the multidimensional potential energy surface.

A much larger impact parameter was determined in the photodissociation of formaldehyde.[29] Since the experimental conditions were chosen in a way that the initial parent angular momentum is essentially zero, the range of b could be calculated ($L = \mu v b \cong |\mathbf{J}_{CO} + \mathbf{J}_{H_2}|$) after a measurement of the relative velocity v and the rotation of the CO and H_2 products. The CO fragment is formed in high rotational states while J_{H_2} is small. For H_2 ($v = 3$, $J = 6$) and $J_{CO} = 18$ the impact parameter ranges from $b = 29$ pm for a counter-rotation to $b = 61$ pm for a corotation of the products. Hence, this large impact parameter is outside the center of the carbon nucleus. This could be an example where off-diagonal elements of the probability matrix P are significant in the description of the dissociation process.

In conclusion, we have measured the angular momentum pair correlation described by the complete joint reaction probability $P(J_A, J_B)$. In conjunction with the vector correlation between the translational and rotational motion even the vectorial pair correlation is determined quantitatively together with the impact parameter of a fragmentation process where four atoms are involved. This is the most detailed information available on a molecular decay process and a comparison with calculated state-resolved cross sections $\sigma(J_A, J_B)$ is the ultimate test for dynamical theories.

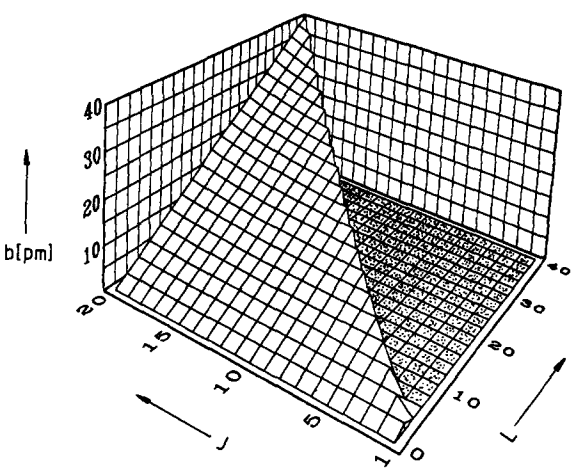

FIG. 8. Possible values of the impact parameter b as a function of product rotation and orbital angular momentum. The shaded area is not accessible because of conservation of angular momentum. In the photodissociation of H_2O_2 at 193 nm $\mathbf{J}_A$ and $\mathbf{J}_B$ essentially point in opposite directions and b is of the order of 1 pm.

ACKNOWLEDGMENTS

The work has been performed as part of a special program of the Deutsche Forschungsgemeinschaft (DFG). Financial support is gratefully acknowledged. We also thank Professor D. E. A. Reinsch for many helpful discussions

related to the hyperfine splitting of OH, and Dr. R. Schinke for sending us the results of trajectory calculations prior to publication.

[1] G. E. Hall and P. L. Houston, Annu. Rev. Phys. Chem. (to be published).
[2] K.-H. Gericke, S. Klee, F. J. Comes, and R. N. Dixon, J. Chem. Phys. **85**, 4463 (1986).
[3] A. U. Grunewald, K.-H. Gericke, and F. J. Comes, J. Chem. Phys. **87**, 5709 (1987).
[4] D. Schwarz-Lavi and S. Rosenwaks, J. Chem. Phys. **88**, 6922 (1988).
[5] M. H. Alexander *et al.*, J. Chem. Phys. **89**, 1749 (1988).
[6] J. H. Shan, V. Vorsa, S. J. Wategaonkar, and R. Vasudev, J. Chem. Phys. **90**, 5493 (1989); R. Vasudev, R. N. Zare, and R. N. Dixon, *ibid.* **80**, 4863 (1984).
[7] F. Shokoohi, S. Hay, and C. Wittig, Chem. Phys. Lett. **110**, 1 (1984); I. Nadler, D. Mahgerefteh, H. Reisler, and C. Wittig, J. Chem. Phys. **82**, 3885 (1985).
[8] H. Joswig, M. A. O'Halloran, R. N. Zare, and M. S. Child, Faraday Discuss. Chem. Soc. **82**, 79 (1987).
[9] J. C. Stephenson, M. P. Casassa, and D. S. King, J. Chem. Phys. **89**, 1378 (1988); B. R. Foy, M. P. Casassa, J. C. Stephenson, and D. S. King, *ibid.* **89**, 608 (1988); M. H. Alexander, H. J. Werner, and P. J. Dagdigian, *ibid.* **89**, 1388 (1988).
[10] A. Ticktin and J. R. Huber, Chem. Phys. Lett. **156**, 372 (1989).
[11] D. C. Dayton, K. W. Jucks, and R. E. Miller, J. Chem. Phys. **90**, 2631 (1989).
[12] D. Eres, M. Gurnick, and J. D. McDonald, J. Chem. Phys. **81**, 5552 (1984).
[13] K.-H. Gericke, A. U. Grunewald, S. Klee, and F. J. Comes, J. Chem. Phys. **88**, 6255 (1988).
[14] C. Maul, H. Gläser, and K.-H. Gericke, J. Chem. Soc. Faraday Trans. 2 **85**, 1297 (1989).
[15] R. N. Dixon, J. Nightingale, C. M. Western, and X. Yang, Chem. Phys. Lett. **151**, 328 (1988).
[16] Z. Xu, B. Koplity, and C. Wittig, J. Chem. Phys. **90**, 2692 (1989).
[17] K.-H. Gericke, Phys. Rev. Lett. **60**, 561 (1988).
[18] U. Brühlmann, M. Dubs, and J. R. Huber, J. Chem. Phys. **86**, 1249 (1987); M. P. Docker, A. Ticktin, U. Brühlmann, and J. R. Huber, J. Chem. Soc. Faraday Trans. 2 **85**, 1169 (1989).
[19] A. U. Grunewald, K.-H. Gericke, and F. J. Comes, J. Chem. Phys. **89**, 345 (1988).
[20] M. Nuß, K.-H. Gericke, and F. J. Comes, J. Quant. Spectrosc. Radiant. Trans. **27**, 191 (1982).
[21] G. H. Dieke and H. M. Crosswhite, J. Quant. Spectrosc. Radiant. Trans. **2**, 97 (1962).
[22] S. Gerstenkorn and P. Luc, *Atlas du Spectre d'Absorption de la Molecule d'Iode* (Centre National de la Recherche Scientifique, Paris, 1978).
[23] W. Siebrand, W. L. Meerts and D. W. Pratt, J. Chem. Phys. **90**, 1313 (1989).
[24] W. L. Meerts, Chem. Phys. Lett. **46**, 24 (1977); J. L. Destombes, C. Marliére, A. Beanudry, and J. Brillet, Astron. Astrophys. **60**, 55 (1977).
[25] J. J. terMeulen, G. W. M. van Mierlo, and A. Dymanus, Phys. Rev. Lett. **43**, 29 (1979).
[26] E. A. Reinsch (private communication).
[27] Schinke, J. Phys. Chem. **92**, 4015 (1988).
[28] R. Schinke and V. Staemmler, Chem. Phys. Lett. **145**, 486 (1988).
[29] T. J. Butenhoff, K. L. Carleton, M. C. Chuang, and G. B. Moore, J. Chem. Soc. Faraday Trans. 2 **85**, 1155 (1989).